

national accelerator laboratory

NAL-Pub-73/26-EXP
7200.141

ANL/HEP 7316

(Submitted to Phys. Rev. Letters)

INCLUSIVE π^- DISTRIBUTIONS FROM 205 GeV/c pp INTERACTIONS

Y. Cho, R. Engelmann, T. Fields, L. Hyman, and R. Singer
Argonne National Laboratory, Argonne, Illinois 60439 USA

and

L. Voyvodic and J. Whitmore
National Accelerator Laboratory, Batavia, Illinois 60510 USA

June 1973



Inclusive π^- Distributions from 205 GeV/c pp Interactions

Y. CHO, R. ENGELMANN*, T. FIELDS, L. HYMAN and R. SINGER
Argonne National Laboratory, Argonne, Illinois 60439

and

L. VOJVODIC and J. WHITMORE
National Accelerator Laboratory, Batavia, Illinois 60510

Inclusive π^- distributions from 205 GeV/c pp interactions, covering the full range of longitudinal and transverse momenta, have been obtained using the 30-inch hydrogen bubble chamber at NAL. These data provide new evidence for scaling in the fragmentation region and for a plateau in the central region of rapidity. The 90° CM invariant cross section varies as $e^{-(10 \pm 2) P_T^2}$ in the range $P_T^2 \leq 0.1$ (GeV/c)².

*Present Address: Physics Department, State University of New York, Stony Brook, New York 11790.

In this Letter, we report on a measurement of the single particle inclusive distribution for the reaction $pp \rightarrow \pi^- + \text{anything}$ at 205 GeV/c. This measurement covers the entire range in both the center of mass longitudinal (P_L^*) and transverse (P_T) momenta. This is also the highest energy at which a single experiment covering the entire range of these variables has been reported. Similar data^(1, 2) have been reported from the CERN Intersecting Storage Rings (ISR). These ISR experiments cover various restricted intervals of P_L^* and P_T , at energies corresponding to laboratory momenta between 225 and 1500 GeV/c.

Our data were obtained from approximately 17,000 pictures taken with the 30-inch hydrogen bubble chamber exposed to a 205 GeV/c proton beam at the National Accelerator Laboratory (NAL). The results reported here are confined to negative particle production. Ordinarily, the measurement of momenta and angles of secondary tracks in a bubble chamber is a routine matter. However, for this high beam momentum and for high multiplicity events, there are practical complications involving track matching in the different stereoscopic views, overlapping track images, and poor momentum determination for fast forward-going secondaries. To determine how these complications might affect our data, we have made two independent sets of measurements, using somewhat different experimental methods.

Following the scan⁽³⁾ of the film, a fiducial volume was selected that yielded a 20 cm minimum track length for outgoing tracks. For the first measurement method, each view was examined at high magnification (6 times

life size), and the spatial pattern of the bubbles used to match all secondary tracks. The event was then measured in two views and spatially reconstructed using TVGP. For the second method, a minimum sagitta criterion was used to determine which negatively charged secondary tracks were candidates for production in the backward CM hemisphere.⁽⁴⁾ These tracks were then measured in three views and processed through TVGP, using a computer track matching program. The numbers of events (negative tracks) analyzed by each method were 440(1250) and 1484(1854), respectively. The two methods yielded compatible results in a track-by-track test as well as compatible distributions for the entire samples, and the data have been combined.

Typical measurement errors in $y^* = \tanh^{-1}(P_L^*/E^*)$, P_T , and $x = 2P_L^*/\sqrt{s}$ were also determined by repeated measurements of a sample of the events. For 40 GeV/c negative tracks ($x \approx +0.2$; 95% of the negative tracks have lower momenta), typical errors are $\Delta y^* \sim 0.2$, $\Delta P_T \sim 0.1$ GeV/c, and $\Delta x \sim 0.03$. These, as well as the smaller errors associated with backward hemisphere and 90° CM tracks, provide ample resolution for the spectra presented here.

Since pp collisions are symmetric in the CM system, the backward hemisphere is equivalent, for single particle spectra, to the entire solid angle. This symmetry may be used to check the track selection and measurements for the above two methods. However, to exploit this symmetry and to calculate kinematic quantities (e. g., rapidity) on an individual track

basis require mass identification, which we do not have.

Since the negative tracks are mostly pions, we have used a simple Monte Carlo technique to estimate the effects of the K^- and \bar{p} contamination. We tried several functional forms for the K^- and \bar{p} spectra with intensities⁽⁵⁻⁷⁾ of 7% K^- 's and 2% \bar{p} 's in the Monte Carlo generation. The resulting corrections⁽⁸⁾ were insensitive to reasonable variations of the shape of the K^- and \bar{p} spectra.

Fig. 1 shows the π^- invariant cross section $E \frac{d^3\sigma}{dp^3}$ as a function of x for different values of P_T .⁽⁹⁾ Also shown are published data at 28.5 GeV/c⁽¹⁰⁾ and at ISR energies.^(1,2) For $|x| \geq 0.1$, the data are consistent with scaling behavior at 205 GeV/c. Furthermore, for larger $|x|$, scaling may extend down to less than 30 GeV/c.

Fig. 2 shows $E \frac{d^3\sigma}{dp^3}$ as a function of P_T^2 for $|x| \leq 0.02$,⁽¹¹⁾ as well as the integral with respect to x of the invariant cross section. The integrated distribution at 205 GeV/c is very similar to the distribution observed⁽¹⁰⁾ at 28.5 GeV/c. Our $|x| \leq 0.02$ ($\sim 90^\circ$ CM) data are in good agreement with ISR data⁽²⁾ for $x \cong 0$ and $P_T \geq 0.23$ GeV/c. The solid curve is given by $146 \exp(-6.39 P_T + 0.36 P_T^2)$ and is taken from the fit of Banner et al.⁽²⁾ to their $\sqrt{s} = 23.2$ GeV data. The extrapolation of this curve into the region $P_T < 0.23$ GeV/c is also shown. It is clear that the extrapolated curve lies considerably above our data points.

In the range $P_T^2 \leq 0.1$ (GeV/c)², our 90° invariant cross section is

well fit by $(55 \pm 4) e^{-(10 \pm 2)P_T^2}$. A similar gaussian behavior at small P_T (for $x \approx 0.2$) has previously been observed at 12 GeV/c by Akerlof et al. ⁽¹²⁾ and at 24 GeV/c by Allaby et al. ⁽¹³⁾ In these low energy experiments, the data are not consistent with an $\exp(-BP_T)$ variation at small P_T . Our 90° CM data also favor a gaussian variation at small P_T , and are inconsistent with the exponential behavior at small P_T given by the extrapolation of the fit of Banner et al. ⁽²⁾

The small P_T region is quite important in determining the behavior of $\frac{1}{\pi} \frac{d\sigma}{dy}$ in the central region as a function of s . The region $P_T^2 \leq 0.05$ (GeV/c)², according to our data, contains $\sim 33\%$ of the 90° cross section.

Integrating our data over P_T^2 , we obtain

$$\frac{1}{\pi} \left(\frac{d\sigma}{dy} \right)_{y^*=0} = (6.5 \pm 0.5) \text{ mb} .$$

The fit of Banner et al. to their ISR data, when integrated over all P_T , gives $\frac{1}{\pi} \left(\frac{d\sigma}{dy} \right)_{y^*=0} = (7.7 \pm 0.5) \text{ mb}$. However, if the form $A \exp(-BP_T^2) + C \exp(-DP_T^2)$, which is consistent with both our data and low energy data, were used with the data of Banner et al., the 90° cross section would decrease by $\sim 15\%$. Therefore, conclusions regarding scaling behavior of the ISR integrated 90° cross section are correspondingly uncertain.

In Fig. 3 we present our rapidity distributions for various multiplicities. ⁽¹⁴⁾ There is a definite trend ⁽¹⁵⁾ for the width of the distribution to decrease as the multiplicity increases. The RMS width of the highest

multiplicity data shown in Fig. 3 is a factor of 1.3 ± 0.1 smaller than that of the lowest multiplicity data.

Fig. 4 shows the π^- inclusive rapidity distribution (summed over all multiplicities) and a comparison with the 28.5 GeV/c data. Because of the above inconsistency between our results at low P_T and the P_T parameterization used for some of the ISR data, we have not shown integrated ISR results in Fig. 4.

From the rapidity data shown in Fig. 4, we note that:

1. The scaling of the invariant cross section $E \frac{d^3\sigma}{dp^3}$ in the fragmentation region appears as scaling for $\frac{1}{\pi} \frac{d\sigma}{dy}$ for $y_{\text{Lab}} \leq 1$ and seems to occur at energies less than 30 GeV/c. In this y region, our $\frac{d\sigma}{dy}$ results are equal to those at 28.5 GeV/c within the experimental precision of $\sim \pm 10\%$.
2. Our data show evidence for a plateau in the central region. The full width of the plateau is of the order of two units of rapidity. In fact, even the separate multiplicity curves in Fig. 3 are individually consistent with such a plateau.
3. $d\sigma/dy$ for π^- in the central region is increasing with s ; i. e., scaling, if it occurs in this region, is being approached from below.

Finally, it is interesting to point out that Landau's hydrodynamical model⁽¹⁶⁾ is not ruled out by the inclusive distributions shown here. This model predicts a gaussian distribution in rapidity and provides an adequate

description of our data.

We wish to thank the 30-inch bubble chamber crew and the staff of the neutrino laboratory at NAL for their help in obtaining this exposure. We are also extremely grateful to the scanning and measuring personnel at both Argonne and NAL for their conscientious efforts. Finally, it is with pleasure that the NAL authors and R. Engelmann acknowledge most informative discussions with E. L. Berger and M. Jacob in the early stages of this analysis.

References

1. A. Bertin et al., Phys. Letters 38B, 260 (1972).
2. M. Banner et al., Phys. Letters 41B, 547 (1972).
3. G. R. Charlton et al., Phys. Rev. Letters 29, 515 (1972).
4. For pion production at 90° CM, the maximum laboratory momentum is 15 GeV/c, assuming a transverse momentum limit of 1.45 GeV/c.
5. G. R. Charlton et al., Phys. Rev. Letters 30, 574 (1973). They find $2\sigma(K_S^0)/\sigma(\pi^-) = 0.17 \pm 0.02$.
6. M. G. Albrow et al., Phys. Letters 40B, 136 (1972).
7. A. Bertin et al., Phys. Letters 41B, 201 (1972).
8. The resulting π^- fraction as a function of y in the backward CM hemisphere ranges from 0.90 to 0.98. In the forward hemisphere, the pion

contribution varies from 0.91 at 90° to ~ 0.70 in the beam fragmentation region. After applying these corrections, our distributions are consistent with forward-backward CM symmetry.

9. For purposes of comparison, we show our data for the following P_T^2 intervals: (0, 0.08), (0.12, 0.20) and (0.4, 0.7) $(\text{GeV}/c)^2$.
10. W. H. Sims et al., Nucl. Phys. B41, 317 (1972) and J. Hanlon, private communication.
11. We have also tried using rapidity ($|y^*| \leq 0.8$) rather than x to select a region near 90° CM. The results were unchanged by this procedure or by narrowing the x or y^* interval.
12. C. W. Akerlof et al., Phys. Rev. D3, 645 (1971).
13. J. V. Allaby et al., Contribution to the Fourth International Conference on High Energy Collisions, Oxford, United Kingdom (1972).
14. The results of Ref. 5 indicate that the kaon fraction is roughly independent of multiplicity. We also assume a similar behavior for \bar{p} .
15. Preliminary indications of this trend have been reported by J. Whitmore et al. and G. Bellettini et al. in Proceedings of the XVI International Conference on High Energy Physics, (Ed. J. D. Jackson and A. Roberts) Vol. I (1972).
16. S. Z. Belenkji and L. D. Landau, Suppl. Nuovo Cimento 3, 15 (1956);

P. Carruthers and M. Duong-Van, Phys. Letters 41B, 597 (1972);

F. Cooper and E. Schonberg, Phys. Rev. Letters 30, 880 (1973).

FIGURE CAPTIONS

- Fig. 1 The inclusive π^- invariant cross section as a function of x for different P_T values. All cross sections given in this paper refer to only one hemisphere, and must be integrated over both hemispheres to obtain total cross sections.
- Fig. 2 Inclusive π^- invariant cross section at 90° CM as a function of P_T^2 . Also shown is the invariant cross section integrated from $x = 0$ to $x = 1$.
- Fig. 3 The π^- rapidity distributions for various charged multiplicities.
- Fig. 4 The inclusive π^- rapidity distribution at 205 GeV/c. The curve represents the 28.5 GeV/c data.

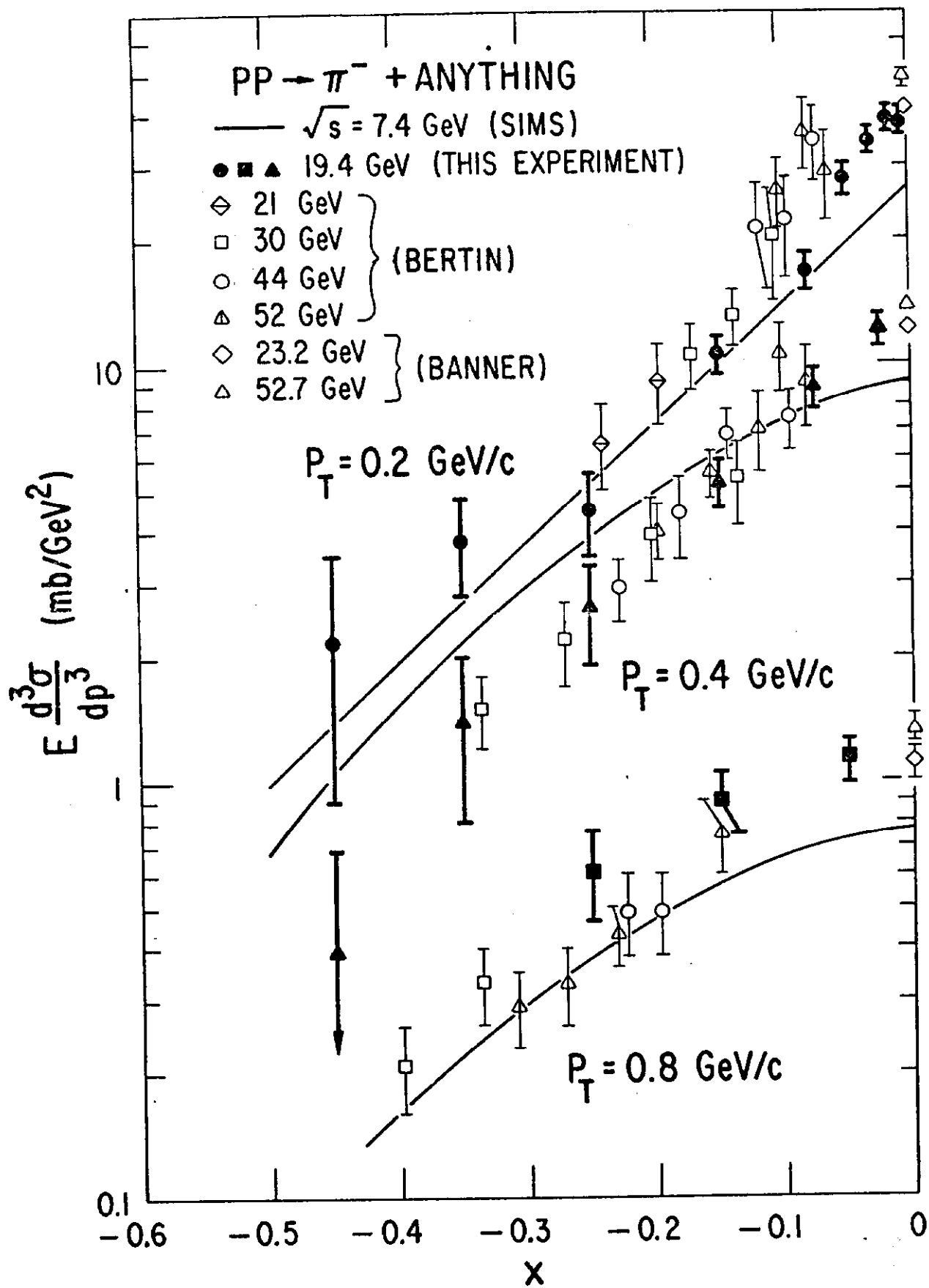


Fig. 1

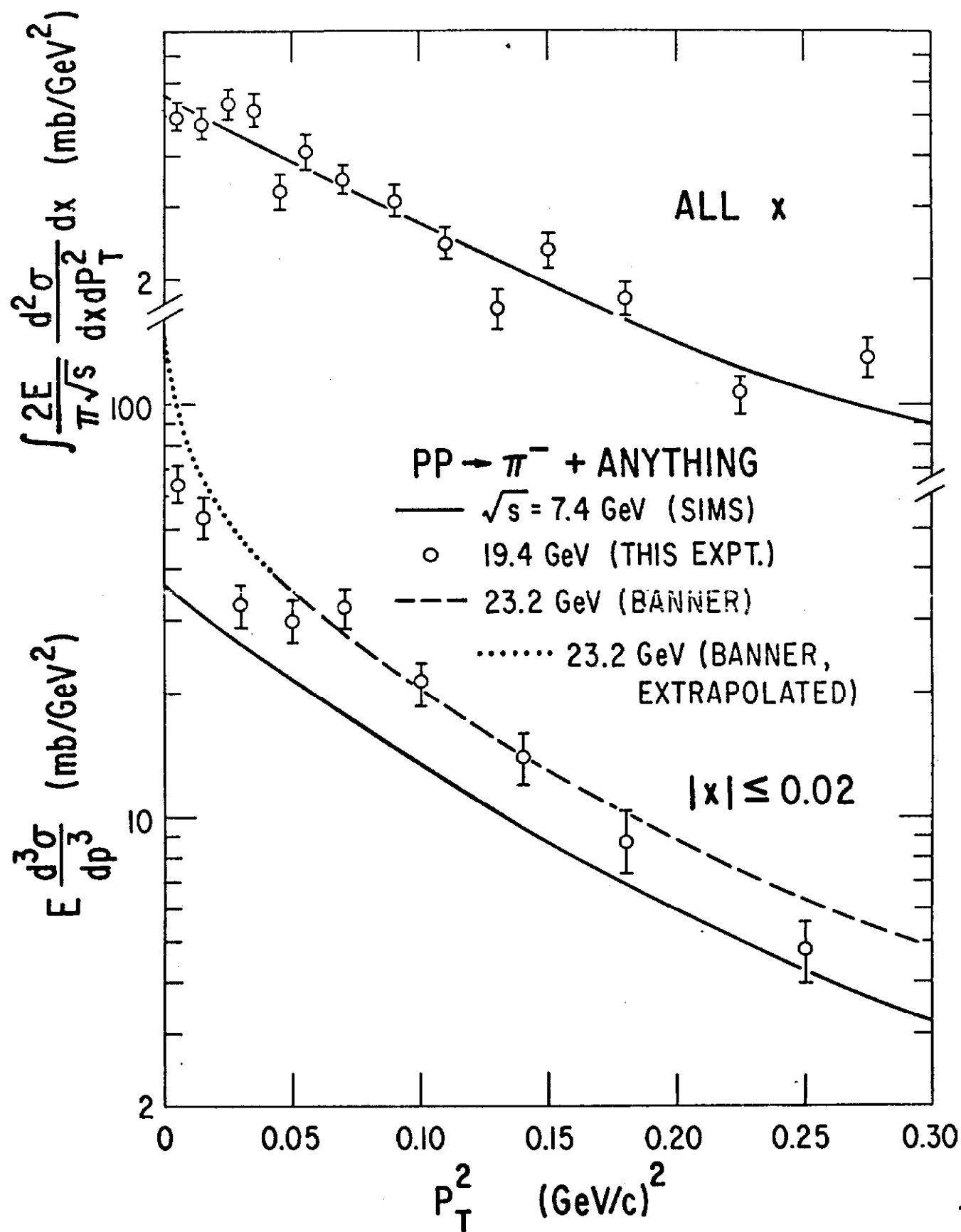


Fig. 2

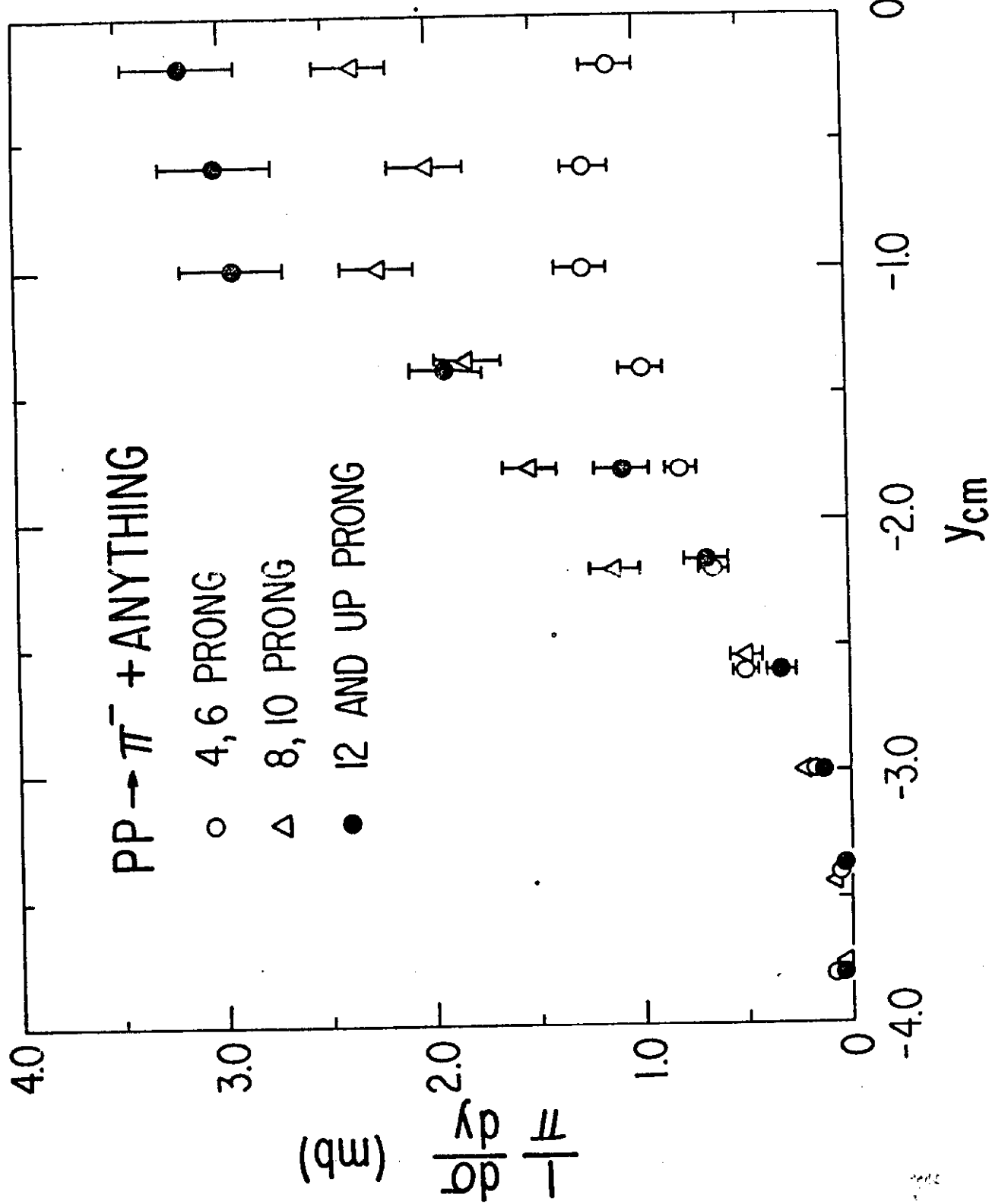


Fig. 3

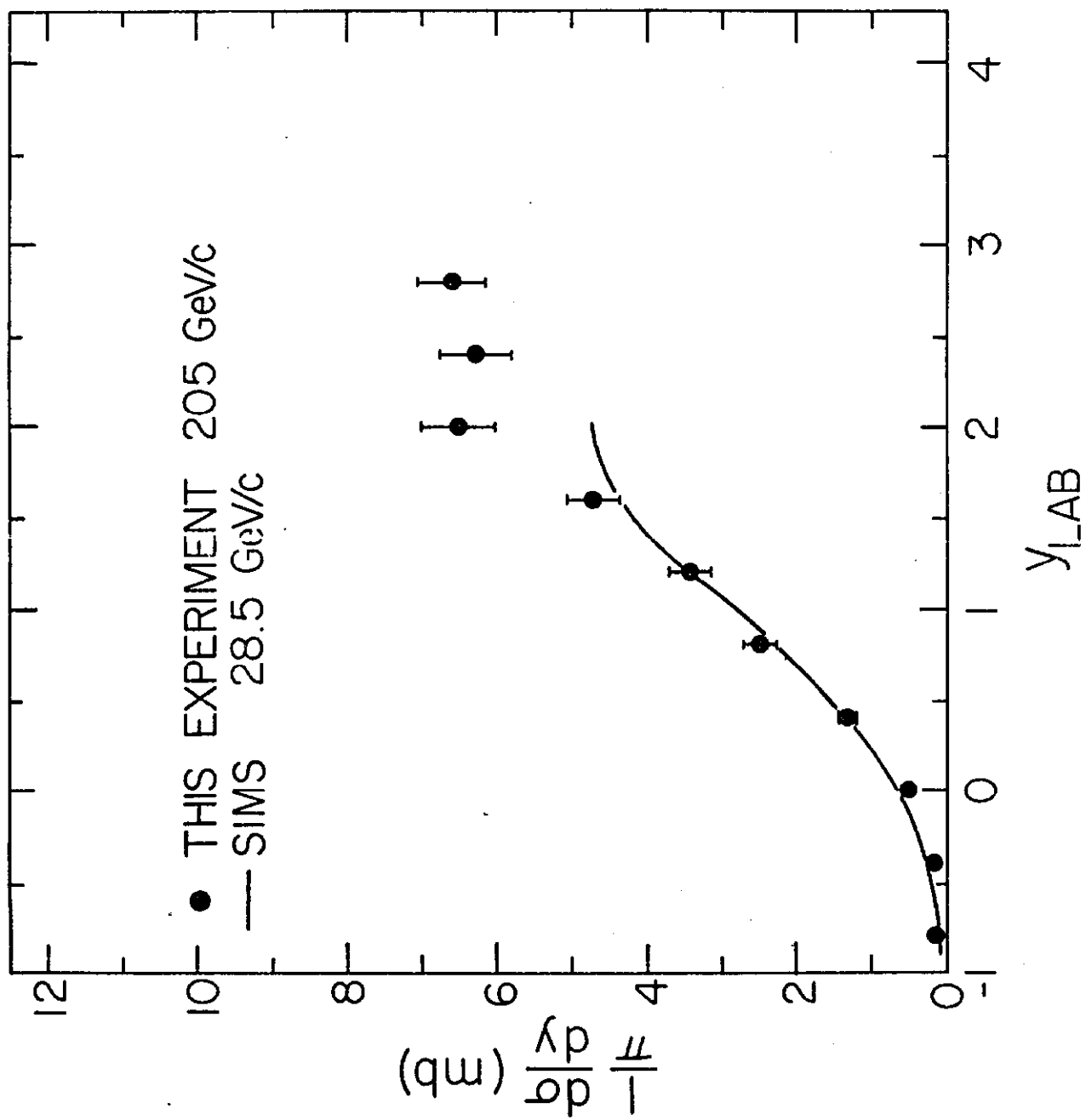


Fig. 4